ChemComm

Accepted Manuscript

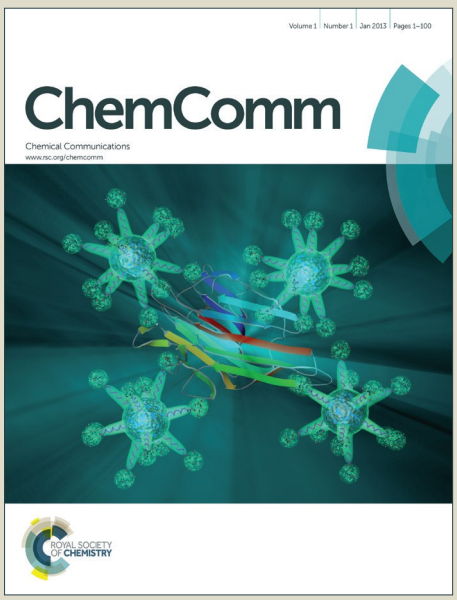

ROYAL SOCIETY OF CHEMISTRY

www.rsc.org/chemcomm

Journal Name

COMMUNICATION

Hierarchically core/shell-structured titanosilicate with multiple mesopore systems for highly efficient epoxidation of alkenes

Received 00th January 20xx,
Accepted 00th January 20xx

DOI: 10.1039/x0xx00000x

www.rsc.org/

Chen-Geng Li, Yiqun Lu, Haihong Wu, Peng Wu* and Mingyuan He*

A hierarchical titanosilicate, with epitaxially grown MFI nanosheets on microsized TS-1 crystals, has been prepared through a desilication-recrystalization method with diammonium surfactant as a secondary structure-directing agent (SDA). This core/shell material is featured by multiple mesoporosities, significantly improved epoxidation activity as well as easy separation in synthesis and catalytic reactions.

TS-1 zeolite has experienced a golden age since its discovery in 1980s.[1-5] The large surface area, high adsorptive capacity, suitable hydrophobicity, intersected 10-MR channels and active Ti sites render this catalyst useful for a variety of liquid-phase reactions with H_2O_2 as oxidant such as selective oxidation of alkenes and alkanes,[6,7] ammoximation of ketones,[8] hydroxylation of aromatics.[9] In its further exploration, TS-1 is facing the troubles of micropore-imposed mass transfer resistance with bulk crystals as well as separation difficulties in hydrothermal synthesis and slurry reactors with nanosized crystals.

The applications of TS-1 are expected to be broadened greatly when the diffusion path length of its micropores is reduced. In this sense, MFI nanosheets with unit-cell thickness have been syntheisized by employing Gemini-type diammonium surfactants as SDAs.[10,11] The ultrathin nanosheet structure minimizes the diffusion pathway to the least, provides high external surface area and large intersheet mesopore volume, and then enhaces the catalytic activity towards bulky substrates.[12] However, the layered TS-1 thus prepared is not compatible with conventional nanosized one in the selective oxidation of small substrates.[10,11] In addition, the high cost of SDA limits the potential of such material. It is highly desirable to minimize the use of expensive SDA.

Decreasing crystal size is one of promising solutions for improving the catalytic performance of TS-1.[13-15] The zeolite crystal size could be limited down to nanoscale by adding extra organic SDA or employing crystal seeds and organosilanes as silicon source in hydrothermal synthesis. Despite an outstanding improvement in activity, the high manufacturing costs hinder wide applications of nanoszied TS-1. Moreover, the nanosized crystals suffer definitely handling and separation problems.

Desilication proves effective to enhance the catalytic ability of zeolites.[16-19] A mild treatment with alkaline solution would create intracrystal mesopores, which however is inevitably at the cost of mass loss by approximately 30 - 50 %. Organic SDA-assisted desilication provides an alternative solution. The dissolved framework silicon species are recrystalized back to pristine crystals with the assistance of SDA, forming hierarchical core/shell structures.[20-22] For these micro-mesoporous materials thus prepared, the mismatching between the lattice of core and the walls of mesosilica shell may interrupt partially the porosity interconnection at the core/sell intersection.[23,24] Constructing an epitaxially grown shell would be helpful for relieving the problems encuntered in conventional core/shell materials.

Here we communicate a strategy to improve the catalytic activity of microsized TS-1 crystals by creating a hierarchical structure through a desilication-recrystallization (DR) process, in which the desolved framework species were recrystallized and epitaxially grown onto the surface of pristine bulk crystals with the assitance of Gemini surfactant SDA. Containing both intracrystal mesopores in core and intercrystalline mesopores in the shell of layered MFI zeolite, this unique material showed an elevated catalytic activity in selective alkene epoxidation.

Pristine TS-1, synthesized in a cheap way and with microsized crystals of 8 - 12 μm, shows well-resolved XRD diffractions in the 2θ region of 5-35° characteristic of the MFI topology (ESI, Fig. S1a). In contrast, as-synthesized lamellar TS-1 (LTS-1) exhibits a high-angle pattern of orientedly grown MFI zeolite along *b* axis together with a mesostructure-related diffraction at 1.4° (ESI, Fig. S1c). The core/shell HTS-1, synthesized by $C_{18\text{-}6\text{-}3}$ surfactant-assisted DR method, is featured by a combined pattern of 3-dimentional (3D) TS-1 and

[a] *Shanghai Key Laboratory of Green Chemistry and Chemical Processes, School of Chemistry and Molecular Engineering, East China Normal University, North Zhongshan Road 3663, Shanghai, China. E-mail: pwu@chem.ecnu.edu.cn, hemingyuan@126.com;*

† Electronic Supplementary Information (ESI) available: Details of experimental procedures, material characterization and catalysis performance. See DOI: 10.1039/x0xx00000x

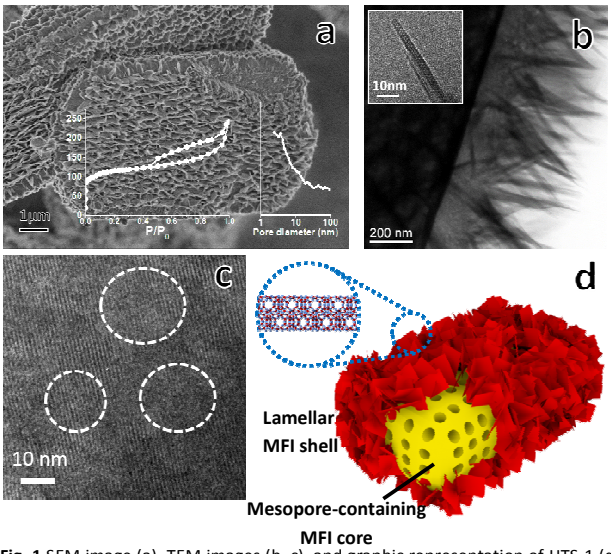

Fig. 1 SEM image (a), TEM images (b, c), and graphic representation of HTS-1 (d). The inset shows the N_2 adsorption/desorption isotherms and pore-size distribution. TEM images show the core/shell intersection, the unilamellar MFI structure in shell as well as the irregular intracrystal mesopores generated by desilication in core crystals.

lamellar TS-1 (ESI, Fig. S1b). Its high-angle diffractions resemble those of 3D TS-1, while an upheaval in low-angle region appears at the same 2θ value as LTS-1, indicative of the presence of the layered mesostructure. In comparison to pure LTS-1, the less intensive layer-related diffraction of HTS-1 is simply because of a low percentage of lamellar MFI phase in this composite material.

The crystal morphology changes obviously after the recrystallization of TS-1 with Gemini surfactant. The pristine TS-1 crystals has a coffin-shaped morphology with a neat external surface (ESI, Fig. S2). After the DR treatment, the TS-1 crystal surface is evenly covered with a shell made up of plate-like phase, forming a core/shell structured material resembling the original coffin-shape (Fig. 1a). The structure of thus prepared HTS-1 was further verified by TEM investigation. The shell is composed of crystalline lamellar zeolite with the thickness of single unit cell (Fig. 1b). The HRTEM image of smashed crystal shows the core was irregularly desilicated, containing randomly distributed intracrystal mesopores (Fig. 1c). Thus, the epitaxial growth of layered MFI on the external surface of TS-1 bulk crystals constructs a hierarchical multiporosity as illustrated in Fig. 1d. For control, TS-1-TPA was prepared by replacing the long-chain Gemini-type SDA with small quaternary ammonium TPABr. The SEM and TEM images reveal that TS-1-TPA possessed a hollow structure inside crystal but without a lamellar structure on the surface (ESI, Fig. 3S and Fig. S4). Although containing intracrystal mesopores like HTS-1, TS-1-TPA possesses a shell merely with a normal microporous MFI structure.

The N_2 adosrption isotherms clearly reveal a significant change in porosity after the different treatment of TS-1 (ESI, Fig. S5). Pristine TS-1 shows a typical type I isotherm characteristic of microporous materials. That of HTS-1 is characteristic of both type I and type IV, implying the presence of multiple pore systems. The slow uptake in the P/P_0 region of

Table 1 Physiochemical properties of various TS-1 catalysts

Cat.	Si/Ti[a]	Si/Na[a]	S_{BET}[b] ($m^2 g^{-1}$)	V_{micro}[c] ($cm^3 g^{-1}$)	V_{meso}[d] ($cm^3 g^{-1}$)	V_{total}[b] ($cm^3 g^{-1}$)	S_{exter}[c] ($m^2 g^{-1}$)
TS-1	46	41(84)	268	0.15	0.02	0.17	14
HTS-1	50	59(49)	339	0.13	0.24	0.37	60
TS-1-TPA	39	13(27)	311	0.22	0.12	0.34	30
TS1-nano	52	∞	368	0.18	0.09	0.27	19
LTS1	25	∞	417	0.16	0.18	0.34	42

[a] Measured by ICP-AES. The numbers in brackets is the Si/Na molar ratios value before washing with HCl.
[b] Calculated from N_2 adsorption isotherms with BET method.
[c] Measured by N_2 adsorption using t-plot method.
[d] $V_{meso} = V_{total} - V_{micro}$.

0.2 - 0.9 is probably because of relatively regular mesopores while the hysteresis loop is presumed to the contribution by the intracrystal mesopores created by desilication. The external surface area increases by four times after the DR procedures in comparison to pristine TS-1 (Table 1). Reasonably, TS-1-TPA also shows an increased mesoporosity but lower in quantity than HTS-1.

The DR UV-Vis spectra indicate that the DR treatments either by Gemini surfactant or TPABr imposed no significant change to the Ti coordination states of TS-1, as the samples still show the main absorbance at 220 nm due to the tetrahedral Ti species (ESI, Fig. S6). Meanwhile, all the samples show in the framework vibration region the characteristic IR band at 960 cm^{-1}, which is attributed to the framework Ti species.[25] The ICP-AES analysis reveals that the overall Si/Ti ratio slightly decreased from 46 to 50 after the DR treatment by Gemini surfactant (Table 1), probably because that a part of leached Ti species were not reassembled back to the TS-1 crystals. The XPS investigation provides the Si/Ti ratio information on the crystal surface. Pristine TS-1 shows in XPS spectrum two intensive Ti 2p bands centered at 464.5 eV and 458.8 eV (ESI, Fig. S6), corresponding to the tetrahedral framework Ti. The surface Si/Ti ratio thus obtained is 25 (ESI, Table S1), lower than the bulk ratio of 46 given by ICP. This indicates the TS-1 crystal surface is slightly rich in Ti. However, the intensity of the same XPS bands drastically decrease and the corresponding surface Si/Ti ratio increases highly to 193 for HTS-1 (ESI, Fig. S6 and Table S1). This is indicative of an ununiform Ti distribution from inside core to outside shell. The reason for Ti loss and different distribution could be explained by a preferential recrystallization of desilicated species. In the process of desilication, there is no preference between Ti and Si since both of them are tetravalent in the framework. Whereas in the process of recrystallization, the Ti species with larger atomic size are less preferred in comparison to the Si species. Thus, Ti and Si are dissolved at similar rates and only Si is favoured by recrystallization, resulting in a Si-rich shell and a gradient distribution of Ti from core to shell. Thus, HTS-1 has a higher Ti content in core while it is nearly of pure silica in shell.

HTS-1 shows in the IR spectrum of hydroxyl stretching region a more intensive band at 3745 cm^{-1} (ESI, Fig. S7), which is attributed to the terminal silanol groups.[26] As comparison, other titanosilicates show a less intensive band at the same position. This indicates that HTS-1 possesses an open external surface as a result of growing layered MFI shell. The conventional TS-1-nano sample directed by TPAOH exhibits broad bands at 3700 cm^{-1} and 3500 cm^{-1}, associated with the internal silanols generated inside or outside the crystals.[27] The extremely small particle size of TS-1-nano gives rise to the framework defects and the silanols with complicated chemical environments. ^{1}H-NMR and ^{29}Si-NMR spectra provide similar information about the silanols (ESI, Fig. S9). All samples show strong signals at -113 ppm in ^{29}Si-NMR spectra and 4.1 ppm in ^{1}H-NMR spectra. The former is associated to the Q^4 $Si(OSi)_4$ species while the later is assigned to physically adsorbed H_2O on zeolite. The resonances at -103 ppm in Si-NMR spectra and at 1.7 ppm in H-NMR spectra are assigned to the silanols.[28,29] The ^{1}H-NMR investigation confirm HTS-1 possesses more silanols than pristine TS-1 and TS-1-TPA. TS-1-nano shows different characteristics as it gives no obvious Si-OH resonance in ^{1}H-NMR spectrum (Fig. S8B, d), while shows a stronger Q^3 signal in ^{29}Si-NMR than other TS-1 samples (Fig. S8A, d). This provides the proof for the existence of internal silanols in TS-1-nano, which contributes little to hydrophilicity. As a result, the DR treatment effectively increases the amount of surface silanol groups, optimizing the hydrophilicity of HTS-1.

The epoxidation of *n*-hexene was first employed as a probe reaction to investigate the catalytic properties of titanosilicates (Table 2). Pristine TS-1 shows the lowest *n*-hexene conversion (9.1 %), indicating the microsized crystals severely limit the intracrystal diffusion for the reactant molecules inside zeolite micropores. Shortening the diffusion path by reducing the particle size would enhance the catalytic performance. Exactly, nanosized TS-1 with raspberry shaped crystals shows an improved conversion of 17.0 %. TS-1-TPA exhibites an activity similar to TS-1-nano. Moreover, the post treatment with TPAOH or TPABr leads to no obvious difference in crystal morphology and catalytic behavior (ESI, Fig. S3 and Table S2). On the other hand, HTS-1 gives 26.1 % *n*-hexene conversion. The DR treatment effectively improves the catalytic performance of titanosilicate, making the microsized crystals even more active than nanosized ones. The formation of lamellar MFI shell benefits the catalytic epoxidation, suggesting the DR treatment is superior to crystal size reducing. However, it seems that the lamellar phase in shell itself is not the active component for the reaction. Firstly, it is because that the aforementioned XPS investigation indicates that HTS-1 is almost free of Ti in lamellar shell. Secondly, LTS-1, with a pure lamellar MFI structure, shows a *n*-hexene conversion of 5.4 %. Ryoo et al also observed the same phenomenon, which could be due to the different catalytic activity between external and internal Ti sites.[12] In the catalytic epoxidation of other alkenes with different sizes, the same trends were observed (Fig. 2). All samples show the best catalytic expoxidation performance for propylene with the smallest molecular dimension, and gradually decreases in activity along

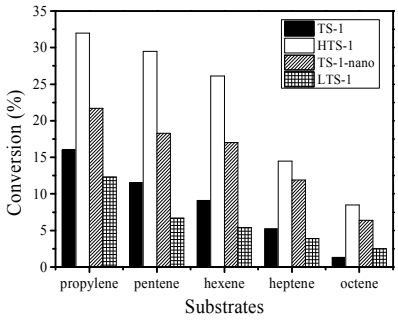

Fig. 2 Epoxidation of various linear alkenes over titanosilicates (Alkene and H_2O_2, 10 mmol; MeOH, 10 mL; cat., 50 mg; temp., 333 K; time, 2 h)

with increasing the molecule size of alkenes. Nevertheless, HTS-1 always appears to be the most active catalyst independent of molecular dimensions.

Recycling experiment was conducted to test the stability of HTS-1. The activity of HTS-1 decreases along with recycling number (ESI, Fig. S11). This could be due to a partial blockage of zeolite channels since the activity of regenerated HTS-1 was recovered to its original level after eliminating the organic residue. This demonstrates that HTS-1 is stable enough in the liquid-phase epoxidation of alkenes. In addition, the core-shell structure is well-preserved for used HST-1 (ESI, Fig. S12).

The reason for the catalytic performance improvement by the DR treatment is considered focusing on the mesoporosity. It is worth noticing that no significant enhancement was observed in the catalytic activity towards the epoxidation of cyclohexene (Table 2). Due to the large size of cyclic substrate, this reaction may take place predominately outside of the 10-MR micropores of MFI structure, that is on the external crystal surface as well as in the secondary mesopores inside crystals or shell generated by the DR treatment. Nevertheless, the shell of HTS-1 contains almost no active sites of Ti species. All these results suggest that the external surface of HTS-1 is almost catalytically inactive. Moreover, the epoxidation in the presence of poisoning agents was performed to detect where the Ti active sites were located. Trimethylamine (TMA)

Table 2 Catalytic epoxidation of linear and bulky alkenes over titanosilicates

Cat.	*n*-Hexene conv. (%) /TON	Cyclohexene conv. (%)	Poisoning oxidation of *n*-hexene (%)			
			TMA		TPhA	
			conv.	sel.	conv.	sel.
TS-1	9.1/50	0.2	0.9	99.2	6.6	99.1
HTS-1	26.1/157	3.5	5.6	98.7	22.1	99.1
TS-1-TPA	22.8/107	1.2	2.8	99.0	13.7	98.8
TS-1-nano	17.0/106	1.6	4.0	99.7	14.8	99.2
LTS-1	5.4/16	2.4	-	-	-	

Reaction conditions: *n*-hexene or cyclohexene, 10 mmol; H_2O_2, 10 mmol; solvent, MeOH for *n*-hexene and MeCN for cyclohexene, 10 mL; amine, if added, 2 mmol; cat., 50 mg; temp., 333 K; time, 2 h. Turnover number (TON) is calculated as the converted alkene molecules per Ti site.

molecules smaller than the 10-MR pores could reach the most of Ti sites while the bulky molecules of triphenylamine (TPhA) are only able to poison the Ti sites on external surface or inside mesopores.[30] As shown in Table 2, the catalytic activity slightly decreases after the poisoning with TPhA while drastically diminishes after overall poisoning with TMA. These results reveal that the active sites for *n*-hexene epoxidation are mostly from the Ti species inside the micropores. Thus, it is reasonable to infer that the improvement of catalytic activity is not directly contributed by the reaction taking place on the mesopores either insider core crystals or layered MFI shell. Taking into consideration that the catalytic activity of zeolites are in a close correlation with their mesopore volumes and external surface area, the shortening of diffusion path should be one of the decisive factors to the reaction.

Alkali-assisted desilication is well known to inevitably generate silanol groups in zeolite framework, so does the recrystallization of the shell with a lamellar structure. Companied with the construction of hierarchical composite structures, the hydrophilicity of the material would be modified. As a result of enrichment in silanol groups, the zeolite hydrophilicity would increase.[31] Hydrophilicity may acts as a two-edged blade to the catalytic reactions. It helps to enrich inside pores the protic reactant molecules like H_2O_2.[32] On the other hand, the water molecules from aqueous H_2O_2 would absorb easily onto the hydrophilic surface and internal silanols, blocking the Ti sites and their accessibility to alkene molecules. In TS-1-nano, a large quantity of internal silanol groups exist in the same crystal as the Ti active sites. Though the diffusion path is reduced to a nanosized length, a high hydrophilicity-induced channel blocking limits the accessibility of Ti sites. Whereas in HTS-1, the core/shell hierarchical structure delicately avoids this disadvantage. The abundant surface silanol groups are helpful for enriching H_2O_2 while the broadened external surface area and mesopores provide open entrances for H_2O_2 and alkene molecules, allowing them to diffuse into Ti-containing core.

The time-dependent synthesis of HTS-1 was carefully traced during 120 h deslication-recrestallization process. The SEM investigation and N_2 adsorption measurement are in agreement with each other (ESI, Fig. S13, Fig. S14 and Table S3), verifying that the epitaxial growth of lamellar MFI shell on TS-1 microsized crystals experiences a mesophase intermediate which is self-assembled from the dissolved Si species by diammonium surfactant. A similar phenomenon has been reported previously in direct hydrothermal synthesis of lamellar MFI zeolite using Gemini-type SDA.[33]

In conclusion, a hierarchical TS-1 has been obtained through a unique desilication-recrystallization with the assistance of Gemini surfactant. The resultant core/shell TS-1 consists of highly crystallized MFI structures both in core and shell but different in long-range extension of framework unit cells. It serves as a more active catalyst for the epoxidation of linear alkenes than other hierarchical or even nanosized TS-1. Such a DR method is helpful to relieve the mass loss of desilication. It is also useful for preparing efficient catalysts of easy separation from less active microsized crystals.

The author gratefully acknowledge the financial support from NSFC of China (21373089) and Programs Foundation of Ministry of Education (2012007613000).

Notes and references

1 M. P. G. Taramasso and B. Notari, US Pat,4410501, 1983.
2 C.S. Cundy and P.A. Cox, *Chem. Rev.*, 2003, **103**, 663.
3 M. G. Clerici, *Top. Catal.*, 2000, **13**, 373.
4 A. Bahn and E. Iglesia, *Acc. Chem. Res.*, 2008, **41**, 559.
5 A. Corma, *Chem. Rev.*, 1997, **97**, 2372.
6 M. G. Clerici and P. Ingallina, *J. Catal.*, 1993, **140**, 71.
7 C. B. Knouw, C. B. Dartt, J. A. Labinger and M. E. Davis, *J. Catal.*, 1994, **149**, 195.
8 J. Le Bars, J. Dakka and R. A. Sheldon, Appl. Catal. A, 1996, **136**, 69.
9 A. Thangaraj, R. Kumar and P. Ratnasamy, J. Catal., 1991, **131**, 294.
10 M. Choi, K. Na, J. Kim, Y. Sakamoto, O. Terasaki and R. Ryoo, *Nature*, 2009, **461**, 246.
11 J. Wang, L. Xu, K. Zhang, H. Peng, H. Wu, J.-G. Jiang, Y. Liu and P. Wu, J. Catal., 2012, **288**, 16.
12 K. Na, C. Jo, J. Kim, W.-S. Ahn and R. Ryoo, *ACS Catal.*, 2011, **1**, 901.
13 T. Degnan, *J. Catal.*, 2003, **216**, 32.
14 W. O. Haag, R. M. Lago and P. B. Weisz, *Faraday Discuss. Chem. Soc.*, 1981, **72**, 317.
15 S. Mintova, J.-P. Gilson and V. Valtchev, *Nanoscale*, 2013, **5**, 6693.
16 P.-Y. Chao, S.-T. Tsai, T.-C. Tsai, J. Mao and X.-W. Guo, *Top. Catal.*, 2009, **52**, 185.
17 N. K. Mal, P. Kumar, M. Sasidharan, M. Matsukata, *Stud. Surf. Sci. Catal.*, 2004, **154C**, 2618.
18 M. Ogura, S. Shinomiya, J. Tateno, Y. Nara, M. Nomura, E. Kikuchi and M. Matsukata, *Appl. Catal. A*, 2001, **219**, 33.
19 J. C. Groen, W. Zhu, S. Brouwer, S. J. Huynink, F. Kapteijn, J. A. Moulijn and J. Perez-Ramirez, *J. Am. Chem. Soc.*, 2007, **129**, 355.
20 D. Wang, L. Xu and P. Wu, *J. Mater. Chem. A*, 2014, **2**, 15535.
21 C. Dai, A. Zhang, L. Li, K. Hou, F. Ding, J. Li, D. Mu, C. Song, M. Liu and X. Guo, *Chem. Mater.*, 2013, **25**, 4197.
22 Y. Zuo, W. Song, C. Dai, Y. He, M. Wang, X. Wang and X. Guo, *Appl. Catal. A*, 2013, **453**, 272.
23 H.-G. Peng, L. Xu, H. Wu, K. Zhang and P. Wu, *Chem. Comm.*, 2013, **49**, 2709.
24 L. Xu, H.-G. Peng, K. Zhang, H. Wu, L. Chen, Y. Liu and P. Wu, *ACS Catal.*, 2013, **3**, 103.
25 M. A. Camblor, A. Corma and J. Perez-Pariente, *J. Chem. Soc., Chem. Comm.*, 1993, **6**, 585.
26 A. Zecchina, S. Bordiga, G. Spoto, D. Scarano, G. Petrini, G. Leofanti, M. Padovan and C. Otero Arean, *J. Chem. Soc., Faraday Trans.*, 1992, **88**, 2959.
27 A. Zecchina, S. Bordiga, G. Spoto, L. Marchese, G. Petrini, G. Leofanti and M. Padovan, *J. Phys. Chem.*, 1992, **96**, 4985.
28 L. Wang, Y. Liu, W. Xie and P. Wu, *J. Phys. Chem. C.,* 2008, **112**, 6132.
29 X. Xue and M. Kanzaki, *Phys. Chem. Miner.*, 1998, **26**, 14.
30 P. Wu and T. Tatsumi, *J. Phys. Chem. B*, 2002, **106**, 748.
31 R. Gounder and M. Davis, *AlChE Journal*, 2013, **59**, 3349.
32 F.-S. Xiao, B. Xie, H. Y. Zhang, L. Wang, X. J. Meng, W. P. Zhang, X. H. Bao, B. Yilmaz, U. Muller, H. Gies, H. Imai, T. Tatsumi and D. De Vos, *ChemCatChem*, 2011, **3**, 1442.
33 K. Na, M. Choi, W. Park, Y. Sakamoto, O. Terasaki and R. Ryoo, *J. Am. Chem. Soc.*, 2010, **132**, 4169.